

Scalable Regularization of Scene Graph Generation Models using Symbolic Theories

Daive Buffelli¹†, Efthymia Tsamoura²

¹ University of Padova

² Samsung AI Research

Several techniques have recently aimed to improve the performance of deep learning models for Scene Graph Generation (SGG) by incorporating background knowledge. State-of-the-art techniques can be divided into two families: one where the background knowledge is incorporated into the model in a subsymbolic fashion, and another in which the background knowledge is maintained in symbolic form. Despite promising results, both families of techniques face several shortcomings: the first one requires ad-hoc, more complex neural architectures increasing the training or inference cost; the second one suffers from limited scalability w.r.t. the size of the background knowledge. Our work introduces a regularization technique for injecting symbolic background knowledge into neural SGG models that overcomes the limitations of prior art. Our technique is model-agnostic, does not incur any cost at inference time, and scales to previously unmanageable background knowledge sizes. We demonstrate that our technique can improve the accuracy of state-of-the-art SGG models, by up to 33%.

Introduction

A *scene graph* is a set of *facts* describing the objects occurring in an image and their inter-relationships. *Scene Graph Generation* (SGG) asks to identify all the facts that hold in an image. Using prior knowledge (for instance commonsense knowledge bases and knowledge graphs (Sap et al. 2019)) is particularly appealing in SGG, as relationships in scene graphs naturally adhere to commonsense principles. This intuition has led to the introduction of *neurosymbolic* techniques (d’Avila Garcez, Broda, and Gabbay 2002) that inject background knowledge into a neural model at training-time and/or use it at inference-time (also called *testing-time*) to amend its predictions.

Neurosymbolic SGG techniques are divided into two major families. The first one represents knowledge in a subsymbolic fashion and incorporates it either only at training-time (Xie et al. 2019), at testing-time (Zareian et al. 2020), or both at training- and testing-time (Gu et al. 2019; Zareian, Karaman, and Chang 2020). The second family maintains knowledge in symbolic form and injects it into the model at training-time only (Donadello, Serafini, and d’Avila Garcez 2017; van Krieken, Acar, and van Harmelen 2019). While

† Work partially done during an internship at Samsung AI Research.

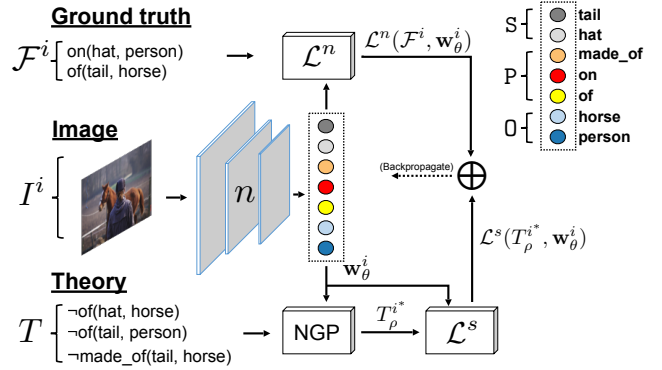


Figure 1: At training-time, background knowledge expressed through negative formulas in first-order logic is injected into a deep model n so that the model’s predictions w_θ^i for each input image I^i adhere to the background knowledge T . Knowledge injection is performed via a logic-based loss function \mathcal{L}^s . To scale to large theories, neural-guided projection (NGP) selects a fixed-size subset T_ρ^{i*} of the theory to compute the loss for each I^i .

they have led to promising results, both groups of techniques face several shortcomings. The first one requires introducing ad-hoc, more complex neural architectures, and accessing the background knowledge at inference-time, thus increasing the training or testing cost. More importantly, ad-hoc neural architectures make it difficult to take advantage of state-of-the-art, neural SGG models, such as VCTree (Tang et al. 2019). The second family suffers from limited scalability with respect to the number of formulas considered, making them impractical in real-world scenarios.

Our work introduces a neurosymbolic regularization technique in which symbolic background knowledge, also referred to as a *theory*, is used as an additional supervision signal for a neural model (see Figure 1). Our objective is to amend the neural network when its predictions do not abide by the background knowledge. The main difference between our proposal and prior art on neurosymbolic SGG is that, instead of providing examples of what the neural model should predict (as in (Gu et al. 2019; Zareian, Karaman, and Chang 2020; Zareian et al. 2020)), we provide examples of

what the model should *not* predict. This is achieved by enforcing negative *integrity constraints (ICs)*, expressed in the form $\neg \text{predicate}(\text{subject}, \text{object})$, through a logic-based loss function. The class of *negative ICs*, which is not supported by (Gu et al. 2019; Zareian, Karaman, and Chang 2020; Zareian et al. 2020) provides two benefits. Firstly, unlike any other symbolic-based regularization method, it allows us to design a technique that scales in the presence of hundreds of thousands of ICs. To this extent, instead of using the whole theory for regularizing every training sample, we propose a *neural-guided projection (NGP)* procedure that identifies a small subset of ICs which are maximally logically violated under the neural predictions. The task of amending the neural module towards having its outputs abide by the ICs amounts to solving an optimization problem in which the weights of the neural module are updated to minimize the maximum violation of the ICs. Secondly, it is easy for users to (semi-)automatically create such ICs from existing knowledge bases or even from the training data itself, by creating a negative IC out of each fact *not* in the knowledge base or training data. To assess the robustness of NGP, we ran experiments using two different theories. The first one was created by taking the complement of the commonsense knowledge graph ConceptNet (Speer, Chin, and Havasi 2017), while the second one by taking the complement of the training facts.

Beyond outperforming prior relevant (sub)symbolic regularization techniques, NGP offers multiple other benefits. Firstly, unlike (Gu et al. 2019; Zareian, Karaman, and Chang 2020), NGP is oblivious to the neural models and loss function used. Furthermore, it does not require accessing the background knowledge at inference-time like (Gu et al. 2019; Zareian, Karaman, and Chang 2020). Similarly to (Xie et al. 2019; Donadello, Serafini, and d’Avila Garcez 2017; Gu et al. 2019; Zareian, Karaman, and Chang 2020; Zhu, Fathi, and Fei-Fei 2014), as well as to prior art on knowledge distillation (Dao et al. 2021; Hinton, Vinyals, and Dean 2015), we do *not* question the background knowledge. Our analysis shows that NGP is robust to the theory in use, improving accuracy even when considering *only* the complement of the training facts as negative ICs. Our empirical comparison confirms that NGP:

- improves the accuracy of state-of-the-art SGG models, namely IMP (Xu et al. 2017), MOTIFS (Zellers et al. 2018) and VCTree (Tang et al. 2019), by up to 33%;
- scales to theories including approximately 1M ICs— sizes no prior symbolic-based regularization technique supports (Donadello, Serafini, and d’Avila Garcez 2017);
- is particularly effective when applied in conjunction with TDE (Tang et al. 2020), a technique that tackles the bias in the data, improving the performance of IMP, MOTIFS and VCTree by up to 16 percentile units;
- outperforms GLAT (Zareian et al. 2020) and LENS (Xie et al. 2019), two state-of-the-art regularization techniques that maintain the knowledge in subsymbolic form, by up to 18% and 15%;
- improves the accuracy of SGG models by up to six times when restricting the availability of ground-truth facts.

Via suitable regularization components, such as TDE (Tang

et al. 2020), we outperform in accuracy recently introduced state-of-the-art models (Li et al. 2021) by up to 90% and ad-hoc neurosymbolic SGG architectures leveraging external knowledge bases (Gu et al. 2019) by up to 86%.

Preliminaries

First-order logic is a language of *predicates*, *variables* and *constants*. *Terms* are either variables or constants. An *atom* α is an expression of the form $p(\vec{t})$, where p is a predicate and \vec{t} is a vector of terms. *Formulas* are expressions composed over atoms and the logical connectives, \wedge , \vee and \neg ; a formula is propositional if instead of atoms, it is composed over terms. A formula is *ground* when it includes exclusively constants. We use $t \in \varphi$ to denote that a variable t occurs in a propositional formula φ . A *theory* T is a set of formulas. The set of all possible atoms formed using the predicates and the constants occurring in T is the *universe* U of T . An *interpretation* J of T is a total mapping from the elements in U to a domain. We denote by $J(\varphi)$ the value of φ in J .

Classical semantics Interpretations J in classical Boolean logic map elements in the universe to either true (\top) or false (\perp). We say that J *satisfies* φ if φ evaluates to true in J , i.e., $J(\varphi) = \top$, and refer to J as a *model* of φ .

Fuzzy logic semantics Interpretations in fuzzy logic map elements in the universe to the interval $[0, 1]$. There are multiple ways¹ to define the logical connectives (see (van Krieken, Acar, and van Harmelen 2020)). We say that J *satisfies* φ if $J(\varphi) = 1$.

Probabilistic semantics In probabilistic logics, similarly to the classical case, statements are either true or false. However, a probability is assigned to these truth values (Hájek, Godo, and Esteva 2013). Consider a propositional formula φ composed over independent Bernoulli random variables, where each variable t is true with probability $p(t)$ and false with probability $1 - p(t)$. Let \mathbf{p} denote the vector of the probabilities so assigned to the variables. The probability $P(J, \mathbf{p})$, of an interpretation J under \mathbf{p} is zero if J is *not* a model of φ ; otherwise it is given by:

$$\prod_{t \in \varphi | J(t) = \top} p(t) \cdot \prod_{t \in \varphi | J(t) = \perp} 1 - p(t). \quad (1)$$

Given (1), the probability of formula φ being true under \mathbf{p} , denoted as $P(\varphi | \mathbf{p})$, is the sum of the probabilities of all the models of φ under \mathbf{p} ((Chavira and Darwiche 2008)):

$$P(\varphi | \mathbf{p}) = \sum_{J \text{ model of } \varphi} P(J, \mathbf{p}). \quad (2)$$

Example 1 Consider the formula $\phi = \neg(h \wedge d \wedge e)$, where h stands for horse, d for drinks and e for eye. All interpretations of ϕ , apart from the one assigning true to each variable, are models of the formula, i.e., the formula evaluates to true in those interpretations. Assuming that each one of the above terms is assigned a probability $p(\cdot)$, the probability of the interpretation that assigns each variable to false is computed as $(1 - p(e)) \times (1 - p(d)) \times (1 - p(h))$.

¹The truth of ground formula φ is: $J(\neg\varphi) := 1 - J(\varphi)$, $J(\varphi_1 \wedge \varphi_2) := \max\{0, J(\varphi_1) + J(\varphi_2) - 1\}$, $J(\varphi_1 \vee \varphi_2) := \min\{1, J(\varphi_1) + J(\varphi_2)\}$ in Lukasiewicz t -(co)norms.

Proposed framework

Scene graph generation aims to identify all the predicate(subject,object) facts that hold in an image. Let S , P and O be the sets of possible subject, predicate and object terms, respectively. Let also n be a neural module that takes an input image and outputs the facts that are predicted to hold in that image. Without loss of generality, we assume that the output neurons of n are divided into three mutually disjoint sets so that there is a one-to-one mapping between the neurons within each set and the elements included in sets S , P and O . We use S , P and O to denote both the sets of terms and the sets of neurons mapped to those terms and use τ to refer both to a term and to the neuron that maps to τ . We denote by $w_\theta(\tau)$ the activation value of output neuron τ , where θ denotes the trainable parameters of n , and by \mathbf{w}_θ the vector of activation values of the output neurons, i.e., the predictions of n .

Facts in a scene graph usually abide by commonsense knowledge. We focus on commonsense knowledge encoded as a theory T in first-order logic and in particular on theories in the form of *integrity constraints* (ICs). Namely, an example of a *negative* IC is the formula φ given by $\neg \text{drinks}(\text{horse}, \text{eye})$, which expresses the restriction that a horse cannot drink an eye. Hereafter, we will consider T to include exclusively *negative, atomic* ICs.

Semantics A theory T can be used to penalize a model n . For instance, penalizing n under φ involves adjusting n 's weights θ so that the neurons `drinks`, `horse` and `eye` cannot *simultaneously* take high activation values. In the language of logic, the terms in S , P and O form a universe. When adopting a probabilistic logic semantics, the activation values \mathbf{w}_θ of the output neurons can be seen as the likelihood $\mathbf{p} = \mathbf{w}_\theta$ of those terms. When adopting the semantics of fuzzy logic, instead, the vector \mathbf{w}_θ can be seen as an interpretation J of the output terms as activation values map terms to the interval $[0, 1]$, see above.

Loss functions

To inject background knowledge into a neural model, we need to quantify the level to which an IC φ is *consistent* with the neural predictions \mathbf{w}_θ . In the case of probabilistic logic, we denote this level of consistency by $P(\varphi|\mathbf{w}_\theta)$ (see (2)). In fuzzy logic, we denote this level of consistency by $\mathcal{L}^s(\varphi)$, as \mathbf{w}_θ is treated as an interpretation. Our framework is not bound to a specific semantics for interpreting theory T , adopting any semantics. To transparently support semantics that blend classical logic with uncertainty, we assume the existence of a function $SAT : (\varphi, \mathbf{w}_\theta) \rightarrow R^+$ expressing the degree of consistency of φ with \mathbf{w}_θ .

Quantifying the consistency between φ and \mathbf{w}_θ allows us to define a loss function $\mathcal{L}^s(\varphi, \mathbf{w}_\theta)$ that is inversely proportional to $SAT(\varphi, \mathbf{w}_\theta)$. Again, we do not stick to a specific loss function or semantics as in prior art, e.g., (Donadello, Serafini, and d'Avila Garcez 2017), but rather spell out the properties a loss function should satisfy to be incorporated into our framework: (i) $\mathcal{L}^s(\varphi, \mathbf{w}_\theta) = 0$ if the probability of φ under \mathbf{w}_θ is one (in the case of probabilistic logic) or $\mathbf{w}_\theta(\varphi) = 1$ (in the case of fuzzy logic); (ii) \mathcal{L}^s is differentiable almost everywhere. The first property is to ensure

the soundness of the loss function w.r.t. the logic semantics, while the second one is to ensure the ability to train via backpropagation. We use $\mathcal{L}^s(T, \mathbf{w}_\theta)$ as a shorthand for $\mathcal{L}^s(\bigwedge_{\varphi \in T} \varphi, \mathbf{w}_\theta)$.

Considered Loss functions

(i) DL2 (Fuzzy logic semantics) We considered the recently introduced fuzzy logic-based loss DL2 (Fischer et al. 2019). The loss is differentiable almost everywhere and its gradients are more effective (i.e., non-zero) than those computed under other fuzzy logics, e.g., PSL (Bach et al. 2017). Below, we recapitulate the definition of DL2.

Definition 1 (Adapted from (Fischer et al. 2019)) Let \mathcal{D} be a set of Boolean variables, X be a variable in \mathcal{D} , φ, φ_1 and φ_2 be formulas over variables in \mathcal{D} and the Boolean connectives \wedge, \vee and \neg , and ψ be the formula that results after applying the De Morgan's rule to formula $\neg\varphi$ until negations are applied on the level of variables. Let also \mathbf{w} be a vector assigning to each variable in \mathcal{D} a value in $[0, 1]$. \mathcal{L}^s is defined as follows:

$$\mathcal{L}^s(X, \mathbf{w}) := 1 - \mathbf{w}(X) \quad (3)$$

$$\mathcal{L}^s(\neg X, \mathbf{w}) := \mathbf{w}(X) \quad (4)$$

$$\mathcal{L}^s(\varphi_1 \wedge \varphi_2, \mathbf{w}) := \mathcal{L}^s(\varphi_1, \mathbf{w}) + \mathcal{L}^s(\varphi_2, \mathbf{w}) \quad (5)$$

$$\mathcal{L}^s(\varphi_1 \vee \varphi_2, \mathbf{w}) := \mathcal{L}^s(\varphi_1, \mathbf{w}) \cdot \mathcal{L}^s(\varphi_2, \mathbf{w}) \quad (6)$$

$$\mathcal{L}^s(\neg\varphi, \mathbf{w}) := \mathcal{L}^s(\psi, \mathbf{w}) \quad (7)$$

(ii) SL (Probabilistic logic semantics) To define a loss based on (2), we can employ standard cross entropy (as in (Tsamoura, Hospedales, and Michael 2021)). The cross entropy of (2) is also known as *semantic loss* (SL) (Xu et al. 2018). An example of the computation of SL is shown in Table 1.

Table 1: Computing the probability of formula $\varphi = \neg(\text{eye} \wedge \text{drinks} \wedge \text{horse})$ for a vector of neural predictions \mathbf{w} . `e` is short for `eye`, `d` is short for `drinks` and `h` is short for `horse`. J denotes a Boolean interpretation of φ .

eye	drinks	horse	$P(J, \mathbf{w})$
\perp	\perp	\perp	$(1 - w(e)) \times (1 - w(d)) \times (1 - w(h))$
\perp	\perp	\top	$(1 - w(e)) \times (1 - w(d)) \times w(h)$
\perp	\top	\perp	$(1 - w(e)) \times w(d) \times (1 - w(h))$
\perp	\top	\top	$(1 - w(e)) \times w(d) \times w(h)$
\top	\perp	\perp	$w(e) \times (1 - w(d)) \times (1 - w(h))$
\top	\perp	\top	$w(e) \times (1 - w(d)) \times w(h)$
\top	\top	\perp	$w(e) \times w(d) \times (1 - w(h))$
\top	\top	\top	0

Properties of loss functions

We summarize some properties for SL (Xu et al. 2018) and DL2 (Fischer et al. 2019). Below, ϕ, ϕ_1, ϕ_2 and \mathbf{w} are as in Definition 1.

Proposition 1 (From (Xu et al. 2018)) *SL satisfies the following properties:*

P_1 . *SL is differentiable almost everywhere;*

- P₂. $SL(\varphi, \mathbf{w}) = 0$, if $P(\varphi, \mathbf{w}) = 1$;
- P₃. $SL(\varphi_1, \mathbf{w}) \leq SL(\varphi_2, \mathbf{w})$, if $P(\varphi_1|\mathbf{w}) \geq P(\varphi_2|\mathbf{w})$;
- P₄. $SL(\varphi_1, \mathbf{w}) = SL(\varphi_2, \mathbf{w})$, if φ_1 is logically equivalent to φ_2 ;

Proposition 2 (From (Fischer et al. 2019)) *DL2 satisfies the following properties:*

- P₁. *DL2 is differentiable almost everywhere;*
- P₂. $DL2(\varphi, \mathbf{w}) = 0$, if $\mathbf{w}(\varphi) = 1$;
- P₃. $DL2(\varphi_1, \mathbf{w}) \leq DL2(\varphi_2, \mathbf{w})$, if $\mathbf{w}(\varphi_1) \geq \mathbf{w}(\varphi_2)$;

While SL satisfies P₄ (this is due to the fact that φ_1 and φ_2 share the same models as they are logically equivalent) DL2 does not satisfy it. We provide an example demonstrating this case. Consider the Boolean formula $\phi_1 = X_1 \wedge X_2 \vee X_1$. Formula ϕ_1 is logically equivalent to the formula $\phi_2 = X_1$ as they both become true whenever X_1 is true. Despite that the probabilities, and consequently the probability-based losses, of both formulas will be the same as they share the same models, the losses computed according to DL2 will be different. The DL2 loss of formula ϕ_1 is computed as $((1 - w(X_1)) + (1 - w(X_2))) \cdot (1 - w(X_1))$, while the DL2 loss of ϕ_2 is computed as $1 - w(X_1)$.

Optimization objective

We are now ready to introduce our technique. Let I^1, \dots, I^m be a sequence of training images. SGG benchmarks such as Visual Genome (VG) (Krishna et al. 2017) include for each image I^i a ground truth set \mathcal{F}^i of predicate(subject,object) facts representing relationships that hold in I^i . State-of-the-art neural modules are trained based on loss functions \mathcal{L}^n that take as arguments the facts in \mathcal{F}^i and the neural predictions for I^i . We denote by \mathbf{w}_θ^i the predictions of n for I^i . As increasing the level of consistency between the ICs in T and \mathbf{w}_θ^i reduces to minimizing the loss function \mathcal{L}^s , our optimization objective becomes:

$$\theta^* := \arg \min_{\theta} \beta_1 \cdot \sum_{i=1}^m \mathcal{L}^n(\mathcal{F}^i, \mathbf{w}_\theta^i) + \beta_2 \cdot \sum_{i=1}^m \mathcal{L}^s(T, \mathbf{w}_\theta^i).$$

Above, β_1 and β_2 are hyperparameters setting the importance of each component of the loss. In our empirical evaluation, those hyperparameters are computed in an automated fashion using (Kendall, Gal, and Cipolla 2018). The loss function can be an arbitrary, non-linear function and hence $\mathcal{L}^s(T, \mathbf{w}_\theta^i)$ is not necessarily equal to $\sum_{\varphi \in T} \mathcal{L}^s(\varphi, \mathbf{w}_\theta^i)$.

Neural-Guided projection

Commonsense knowledge bases can be quite large. Hence, if naively implemented, regularization would be very time consuming if not infeasible. To overcome this limitation in a way that aligns with our optimization objective, for each training image I^i we identify the subset T_ρ^{i*} of ρ integrity constraints associated with the highest value of \mathcal{L}^s among all possible subsets T_ρ^i of ρ ICs. We call the elements of T_ρ^{i*} the *maximally non-satisfied ICs*:

$$T_\rho^{i*} := \arg \max_{T_\rho^i \subseteq T} \mathcal{L}^s(T_\rho^i, \mathbf{w}_\theta^i), \quad (8)$$

Algorithm 1: $NGP(I, \mathcal{F}, T, n_t) \rightarrow n_{t+1}$

- 1: $\mathbf{w} := n_t(I)$
- 2: $T_\rho^* := \arg \max_{T_\rho \subseteq T} \mathcal{L}^s(T_\rho, \mathbf{w})$
- 3: $\ell := \beta_1 \cdot \mathcal{L}^n(\mathcal{F}, \mathbf{w}) + \beta_2 \cdot \mathcal{L}^s(T_\rho^*, \mathbf{w})$
- 4: $n_{t+1} := \text{backpropagate}(n_t, \nabla \ell)$
- 5: **return** n_{t+1}

Note: β_1, β_2 and ρ are hyperparameters.

Algorithm 2: $GREEDY(I, \rho, T, n_t) \rightarrow T^*$

- 1: $\mathbf{w} := n_t(I)$ $T^* := \emptyset$ $j := 1$
 - 2: **while** $|T^*| < \rho$ **do**
 - 3: **get** the j -th $p(s, o)$ prediction maximizing $w(p) \cdot w(s) \cdot w(o)$
 - 4: **if** $\neg p(s, o)$ is in T , **then add** $\neg p(s, o)$ to T^*
 - 5: $j := j + 1$
 - 6: **end while**
 - 7: **return** T^*
-

and regularize the neural module w.r.t. those constraints. Regularizing using the maximally non-satisfied ICs maximizes our chances of providing meaningful feedback to the model. Consider again the IC $\varphi = \neg \text{drinks}(\text{horse}, \text{eye})$. If the likelihood of φ being true under \mathbf{w}_θ is close to zero, then we are confident that the prediction needs to be amended; otherwise, we cannot know whether the neural predictions are indeed the correct ones or not and hence, we cannot provide meaningful feedback. In that case, only the ground truth annotations can provide meaningful supervision signal to the neural model.

Our technique, referred to as *neural-guided projection (NGP)*, is summarized in Algorithm 1, which presents the steps taking place on an image-by-image basis. The algorithm denotes by I the input image, by \mathcal{F} the ground truth facts that hold in I , by T the theory, and by n_t the state of the neural module at the t -round of the training process, while ρ defines the number of ICs to choose. An overview of NGP is shown in Figure 1.

Computing T_ρ^{i*} A greedy strategy for computing the set of maximally non-satisfied ICs is presented in Algorithm 2. The arguments are as in Algorithm 1. Iteratively sampling ρ constraints from the theory and computing \mathcal{L}^s after taking the conjunction of those constraints is also an option.

Proposition 3 summarizes the cases in which the ICs chosen in Algorithm 2 are the ones maximizing (8). Let T^* be the set of ICs returned by Algorithm 2, SL denote the semantic loss and DL2 the fuzzy loss from (Fischer et al. 2019).

Proposition 3 *When $\mathcal{L}^s = SL$, then T^* maximizes (8) when the formulas in T^* share no common variables. When $\mathcal{L}^s = DL2$, then T^* always maximizes (8).*

The proof is based on the notion of linearly-separable logic-based loss functions.

Definition 2 *Let ϕ_1, ϕ_2 and \mathbf{w} be as in Definition 1. A loss function \mathcal{L}^s is linearly-separable if- f $\mathcal{L}^s(\varphi_1 \wedge \varphi_2, \mathbf{w}) = \mathcal{L}^s(\varphi_1, \mathbf{w}) + \mathcal{L}^s(\varphi_2, \mathbf{w})$.*

When \mathcal{L}^s is linearly-separable, then for a theory of closed formulas T , we have

$$\mathcal{L}^s\left(\bigwedge_{\varphi \in T} \varphi, \mathbf{w}\right) = \sum_{\varphi \in T} \mathcal{L}^s(\varphi, \mathbf{w}) \quad (9)$$

Furthermore, we will make use of the following result:

Proposition 4 [From (Xu et al. 2018)] *Continuing with Definition 2, SL is linearly-separable if-ff φ_1 and φ_2 share no common variables.*

We are now ready to return to the main body of the proof.

Proof 1 *We distinguish the following cases:*

Case 1. \mathcal{L}^s is DL2. Firstly, DL2 is linearly-separable due to (5). Furthermore, from (4) and (6), it follows that the loss of an IC $\neg(p \wedge s \wedge o) \equiv \neg p \vee \neg s \vee \neg o$, under \mathbf{w} , will be computed by $w(p) \cdot w(s) \cdot w(o)$. The above, along with the fact that Algorithm 2 chooses the $p(s, o)$ predictions maximizing $w(p) \cdot w(s) \cdot w(o)$ for which $\neg p(s, o)$ is in T , proves Proposition 1.

Case 2. \mathcal{L}^s is SL. From line 3 in Algorithm 2 and from (2), it follows that for a given \mathbf{w} , Algorithm 2 chooses the j -th $p(s, o)$ fact maximizing $P(p \wedge s \wedge o | \mathbf{w})$. Since by definition $P(\top | \mathbf{w}) = 1$, it follows that the chosen prediction minimizes $P(\neg(p \wedge s \wedge o) | \mathbf{w})$, while due to Property P_3 from Proposition 1, it follows that the j -th prediction maximizes $\mathcal{L}^s(\neg(p \wedge s \wedge o), \mathbf{w})$. The above, along with Proposition 4, show that Proposition 1 holds when the formulas in T^* share no common variables.

An example of NGP

We provide an example of NGP applied in conjunction with Algorithm 1 and 2 for greedily computing T_ρ^{i*} .

Example 2 *Consider an input image I^i as in Figure 1, depicting a person wearing a jacket and being in front of a horse. Assume that theory T consists of the following ICs:*

- $\neg \text{drinks}(\text{horse}, \text{eye})$
- $\neg \text{wearing}(\text{horse}, \text{person})$
- $\neg \text{of}(\text{tail}, \text{person})$
- $\neg \text{eats}(\text{person}, \text{jacket})$
- $\neg \text{made_of}(\text{tail}, \text{horse})$
- $\neg \text{made_of}(\text{person}, \text{jacket})$
- $\neg \text{of}(\text{hat}, \text{horse})$

Assume that the six most likely facts returned by the neural model are:

- $\text{of}(\text{tail}, \text{horse})$, with likelihood 0.34.
- $\text{wearing}(\text{horse}, \text{person})$, with likelihood 0.27.
- $\text{looking_at}(\text{person}, \text{tail})$, with likelihood 0.26.
- $\text{made_of}(\text{person}, \text{jacket})$, with likelihood 0.24.
- $\text{wearing}(\text{person}, \text{hat})$, with likelihood 0.19.
- $\text{made_of}(\text{tail}, \text{horse})$, with likelihood 0.19.

Above, the likelihood of each fact is computed by multiplying the neural confidences \mathbf{w} of its constituting subject, predicate, and object, respectively. From the above facts, the ones that not adhering to the theory are

- $\text{wearing}(\text{horse}, \text{person})$,

- $\text{made_of}(\text{person}, \text{jacket})$,
- $\text{made_of}(\text{tail}, \text{horse})$.

Prior art (e.g., (Donadello, Serafini, and d’Avila Garcez 2017)) computes a logic-based loss using all the ICs in the theory, leading to prohibitively expensive computations. Instead, NGP chooses a subset of the ICs, making the computation much more efficient. Assuming $\rho = 2$ in Equation 8 and using the greedy technique from Algorithm 2, NGP will compute a loss by taking only the $\rho = 2$ maximally non-satisfied ICs, see Equation 8. In our example, T_ρ^{i} consists of the following ICs:*

- $\neg \text{wearing}(\text{horse}, \text{person})$
- $\neg \text{made_of}(\text{person}, \text{jacket})$

The logic-based loss function \mathcal{L}^s is computed using T_ρ^{i} and is added to the supervised loss \mathcal{L}^n to obtain the final loss used for training.*

Experiments

Benchmarks Following previous works, e.g., (Zareian, Karaman, and Chang 2020; Li et al. 2021), we use Visual Genome (VG) (Krishna et al. 2017) with the same split adopted by (Tang et al. 2020), and the Open Images v6 (OIV6) benchmark (Kuznetsova et al. 2020) with the same split adopted by (Li et al. 2021). Visual genome (VG) (Krishna et al. 2017) includes 108K images across 75K object and 37K predicate categories. However, as 92% of the predicates have no more than ten instances, we followed the widely adopted VG split containing the most frequent 150 object categories and 50 predicate categories. has in total 126K images for training and 1,813 and 5,322 images for validation and testing. In total, 301 object and 31 predicate categories are included. In both benchmarks, each training, validation and testing datum is of the form (I, \mathcal{F}) , where I is an image and \mathcal{F} is a set of $\text{predicate}(\text{subject}, \text{object})$ facts relevant to I . The objects in each fact in \mathcal{F} are annotated with their surrounding bounding boxes. We mostly focus on VG, as it is heavily biased (Tang et al. 2020) and more challenging than OIV6 (SGG models have lower performance for VG than for OIV6, as also reported in (Li et al. 2021)).

Theories We used VG^\neg and CNet^\neg . VG^\neg was computed by taking the complement of the training facts: we enumerated all combinations of predicates, subjects and objects in VG and for each $p(s, o)$ fact that is *not* in the set of training facts, where p , s and o denotes a predicate, subject and object in the domain of VG, we added to VG^\neg the IC $\neg p(s, o)$. We adopted the same approach to create theory CNet^\neg out of ConceptNet’s knowledge graph. However, there we considered sparse subgraphs of the entire graph. In particular, we identified subject-object pairs (s, o) having less than ten $p(s, o)$ facts in ConceptNet, where p , s and o denotes a predicate, subject and object in the domain of VG or OIV6, respectively. We then repeated the same process for subject-predicate and predicate-object pairs. While the presence, or absence, of a fact in either ConceptNet or the VG training data affects our theory, NGP is not biased by the training facts’ frequencies. We did not manually check the resulting

theories and hence, they may include constraints that violate commonsense, reflecting real-world noisy settings. Theories $CNet^\neg$ and VG^\neg include approximately 500k and 1M ICs.

Models Similarly to (Tang et al. 2020) and (Suhail et al. 2021), we applied NGP on three state-of-the-art neural SGG models: **IMP** (Xu et al. 2017), **MOTIFS** (Zellers et al. 2018) and **VCTree** (Tang et al. 2019). Prior art (Zareian et al. 2020; Tang et al. 2020; Li et al. 2021) also considers **KERN** (Chen et al. 2019) and **VTransE** (Zhang et al. 2017)– we use the more recent model **VCTree**.

Regularization techniques We considered several recently proposed state-of-the-art regularization techniques:

- **TDE** (Tang et al. 2020), a neural-based technique that operates at inference-time and aims at removing the bias towards more frequently appearing predicates in the data;
- **GLAT** (Zareian et al. 2020), a neural-based technique that amends SGG models at inference-time using patterns captured from the training facts;
- **LENSR** (Xie et al. 2019), a neural-based technique that amends SGG models at training-time after embedding the input symbolic knowledge into a manifold;
- **LTNs** (Donadello, Serafini, and d’Avila Garcez 2017), a symbolic-based technique that injects the input symbolic knowledge to an SGG model at training-time;
- **ITR**, our own symbolic-based technique that returns the most-likely prediction not violating any input IC, where the likelihood of a prediction is the product of the confidences of its predicate, subject and object as assigned by a model. ITR is an inference-time counterpart to NGP.

LTNs is a direct competitor to NGP, while **LENSR** and **GLAT** are the neural counterpart to NGP. **TDE** does not use commonsense knowledge and hence it is orthogonal to all the other regularization techniques.

Additional architectures We consider **KBFN** (Gu et al. 2019), a state-of-the-art ad-hoc, architecture accessing **ConceptNet** both at training- and at testing-time; and **BGNN** (Li et al. 2021) a recently-introduced confidence-aware bipartite graph neural network with adaptive message propagation mechanism. In contrast to **IMP**, **MOTIFS** and **VCTree**, **BGNN** cannot be easily integrated with regularization techniques, as it makes use of an ad-hoc data sampling procedure at training-time. Indeed, the authors position **BGNN** as an alternative to models trained with **TDE**, and our empirical comparison manifests that it also does not integrate effectively with **LENSR** and **GLAT**.

Computational environment All experiments ran on a Linux machine with 8 NVidia GeForce GTX 1080 Ti GPUs, 64 Intel(R) Xeon(R) Gold 6130 CPUs, and 256GB of RAM.

Overview of experimental results We considered the standard tasks of *predicate* and *scene graph classification*. Given an input image, and a set of bounding boxes with labels indicating the subjects/objects contained in each bounding box, predicate classification asks to predict the facts that hold in the image. In scene graph classification, the goal is the same, but the bounding boxes are unlabeled. We used the standard measures Mean Recall@ k ($mR@k$) and zero-shot Recall@ k ($zsR@k$) to assess accuracy. $mR@k$ was proposed as a replacement to $recall@k$ to address the data bias issue in SGG benchmarks (Tang et al. 2020, 2019). $zsR@k$

measures $recall@k$ considering only the facts that are in the testing but not the training set (Lu et al. 2016).

We employed NGP with different loss functions. We set the number of constraints (i.e., ρ in Eq. 8) to $\rho = 3$. We found that this value adds minimum computational overhead while improving mR and zsR . We considered the loss functions **DL2** (Fischer et al. 2019) (fuzzy logic) and **SL** (Xu et al. 2018) (probabilistic logic). $NGP(X)$ denotes NGP employed using loss X . All experiments ran using the full theories. **LTNs** were prohibitively slow for the size of our theory: using the same computational resources we used for NGP, it would have taken 4,000 hours for training for just one epoch. As such, we do not report results for **LTNs**.

Table 2 shows the impact of NGP, **LENSR** and **ITR** on **IMP**, **MOTIFS** and **TDE** for theory $CNet^\neg$. Similarly, Table 3 shows the impact of NGP, **GLAT** and **LENSR** for theory VG^\neg . **NGP** and **LENSR** adopt VG^\neg for a fair comparison against **GLAT**, as the latter regularizes SGG models using knowledge mined from the training images. Table 4 studies the integration of **TDE** and NGP on **MOTIFS** and **VCTree** (**TDE** does not support **IMP** (Tang et al. 2020)).

The above results are on the **VG** dataset. Table 5 shows the impact of **NGP(SL)** with $CNet^\neg$ and **TDE** on **MOTIFS** for the **OIv6** dataset when the models are trained with limited access to the ground truth labels. In particular, we remove 0%, 50% and 75% of the ground-truth facts at training-time, while keeping the corresponding images in the training set. As all the baselines we consider require the ground facts to compute a loss \mathcal{L}^n , the above setting leads to discarding each sample that misses ground-truth facts when training a baseline model (both with and without **TDE**). In contrast, when applying NGP, we use only \mathcal{L}^s at training-time when the ground-truth facts are not available. The above setting demonstrates the effectiveness of NGP in weak supervision. We report results for **MOTIFS**, as it was the most challenging to regularize, as discussed below. **OIv6** does not provide zero-shot evaluation and, thus, we report only $mR@k$. Similarly to Table 5, Figure 2 shows the impact of **NGP(SL)** with $CNet^\neg$ on **IMP** and **VCTree** when reducing 10%–50% of the ground-truth facts in **VG**. The task of interest is predicate classification. Again, when the ground-truth facts of an image are missing, \mathcal{L}^s is used to back propagate through the SGG model when regularizing under NGP; images that miss ground-truth facts are ignored in the absence of NGP. For completeness, Figure 2 also shows mR and zsR when using the full training set (0% reduction). Figure 3 reports results on **VG** for the ad-hoc architecture **KBFN** and the model **BGNN**. NGP is applied with $CNet^\neg$ and **KBFN** with **ConceptNet**– **KBFN** does not support negative ICs.

The appendix provides further details including implementation details, results on the integration of **BGNN** with **LENSR** and **GLAT**, and an analysis of the effects of different ρ ’s.

Key conclusions

NGP can substantially improve the recall of SGG models. Table 2 shows that NGP with theory $CNet^\neg$ improves the relative $mR@k$ of **IMP**, **MOTIFS** and **VCTree** up to 25%, 3% and 4.5% on predicate classification; on scene graph classi-

Table 2: Impact of different regularization strategies on models’ accuracy using CNet[⊃]. Results on the VG dataset.

Model	Theory	Reg.	Predicate Classification						Scene Graph Classification					
			mR@			zsR@			mR@			zsR@		
			20	50	100	20	50	100	20	50	100	20	50	100
IMP	-	-	9.26	11.43	12.23	12.23	17.28	19.92	5.57	6.31	6.74	2.04	3.47	3.90
IMP	CNet [⊃]	ITR	9.27	11.44	12.23	12.24	17.30	19.94	5.61	6.35	6.78	2.08	3.50	3.92
IMP	CNet [⊃]	LENSR	10.56	13.16	14.22	12.78	18.31	21.06	0.01	0.01	0.02	0.01	0.01	0.01
IMP	CNet [⊃]	NGP(SL)	11.29	14.22	15.30	12.84	18.75	21.84	6.99	8.45	8.92	2.71	4.48	5.35
IMP	CNet [⊃]	NGP(DL2)	11.62	14.73	15.92	13.13	18.57	21.87	5.58	6.42	6.95	2.17	3.50	3.93
MOTIFS	-	-	12.65	16.08	17.35	1.21	3.34	5.57	6.81	8.31	8.85	0.33	0.65	1.13
MOTIFS	CNet [⊃]	ITR	12.68	16.10	17.39	1.23	3.35	5.57	6.82	8.32	8.85	0.35	0.66	1.13
MOTIFS	CNet [⊃]	LENSR	12.50	15.90	17.20	1.12	3.26	5.37	0.30	0.34	0.36	0.02	0.02	0.02
MOTIFS	CNet [⊃]	NGP(SL)	12.94	16.44	17.76	1.31	3.57	5.74	8.16	10.00	10.54	0.49	1.05	1.58
MOTIFS	CNet [⊃]	NGP(DL2)	7.35	10.52	12.34	0.27	0.67	1.20	4.92	7.99	6.56	0.13	0.24	1.09
VCTree	-	-	13.07	16.75	18.11	1.04	3.28	5.52	9.29	11.42	12.12	0.48	1.37	2.09
VCTree	CNet [⊃]	ITR	13.71	17.27	18.58	1.37	3.80	6.38	9.36	11.49	12.19	0.51	1.40	2.17
VCTree	CNet [⊃]	LENSR	13.53	16.98	18.27	1.33	3.83	5.88	0.0	0.01	0.01	0.02	0.02	0.02
VCTree	CNet [⊃]	NGP(SL)	13.69	17.51	18.92	1.29	3.85	6.04	9.89	11.75	12.35	0.67	1.56	2.44
VCTree	CNet [⊃]	NGP(DL2)	13.86	17.49	18.77	1.16	3.62	5.68	9.41	11.56	12.12	0.49	1.38	2.39

Table 3: Impact of different regularization strategies on model’s accuracy using VG[⊃]. Results on the VG dataset.

Model	Theory	Reg.	Predicate Classification						Scene Graph Classification					
			mR@			zsR@			mR@			zsR@		
			20	50	100	20	50	100	20	50	100	20	50	100
IMP	-	-	9.26	11.43	12.23	12.23	17.28	19.92	5.57	6.31	6.74	2.04	3.47	3.90
IMP	-	GLAT	10.04	12.44	13.30	11.87	17.04	19.72	5.95	6.75	7.17	2.09	3.40	3.82
IMP	VG [⊃]	LENSR	10.51	13.29	14.33	12.40	18.07	21.22	0.01	0.01	0.02	0.01	0.01	0.01
IMP	VG [⊃]	NGP(SL)	11.82	15.16	16.46	12.39	18.18	21.13	7.14	8.60	9.15	2.95	4.62	5.66
MOTIFS	-	-	12.65	16.08	17.35	1.21	3.34	5.57	6.81	8.31	8.85	0.33	0.65	1.13
MOTIFS	-	GLAT	12.82	16.26	17.60	1.26	3.49	5.79	6.84	8.34	8.89	0.32	0.63	1.12
MOTIFS	VG [⊃]	LENSR	12.57	16.09	17.38	1.37	3.41	5.65	0.01	0.01	0.01	0.02	0.02	0.02
MOTIFS	VG [⊃]	NGP(SL)	12.10	15.28	16.54	1.34	3.43	5.47	6.27	7.94	8.42	0.14	0.35	0.55
VCTree	-	-	13.07	16.75	18.11	1.04	3.28	5.52	9.29	11.42	12.12	0.48	1.37	2.09
VCTree	-	GLAT	13.88	17.51	18.90	1.28	3.87	6.43	9.39	11.52	12.20	0.51	1.42	2.17
VCTree	VG [⊃]	LENSR	13.46	17.06	18.49	1.27	3.69	5.98	0.0	0.01	0.02	0.01	0.01	0.01
VCTree	VG [⊃]	NGP(SL)	14.09	17.72	19.08	1.35	3.98	6.36	9.57	11.68	12.49	0.61	1.51	2.39

fication, the improvements are up to 33%, 20% and 6.4%. Table 3 shows that when NGP uses VG[⊃], the relative improvements over IMP, and VCTree further increase to 34% and 5% on predicate classification, and to 36% and 3% on scene graph classification. Table 5 shows that NGP can improve the performance of MOTIFS by 4% in predicate classification, even with fewer ground-truth facts. The results in Table 2 for zsR@k also show that NGP can improve a model’s generalization capabilities of predicting facts that are missing from the training set.

We observe MOTIFS is sensitive to regularization: LENSr always decreases its recall; NGP increases its recall with CNet[⊃], but decreases it when adopting either VG[⊃], see Table 3, or the semantics of fuzzy logic, see Table 2. We conjecture that the decreases are because MOTIFS favors the most frequent predicate for a given subject-object pair in the ground-truth facts. Hence, adding a regularization term that penalizes predictions outside of the training facts may lead to severe overfitting explaining also the drastic drop in zsR@k. Regarding the fuzzy logic semantics, the decrease stresses the limitations of techniques like LTNs that are bound to fuzzy logic. Given the above, we only consider probabilistic logic for NGP hereafter, without discarding the potential of fuzzy logic in other scenarios.

NGP outperforms prior regularization techniques in most scenarios. NGP is the most effective regularization

technique in most cases in Table 2. For instance, regularization of IMP via NGP(SL) leads to up to 25% higher mR@k over ITR on predicate classification. With the exception of MOTIFS, NGP also outperforms GLAT and LENSr in the scenarios in Table 3 leading to up to 20% and 27% higher accuracy in predicate and scene graph classification. The results show that LENSr fails to provide a meaningful loss for training for scene graph classification. Below, we attempt to explain why. In advance of regularization, LENSr learns a manifold \mathcal{M} representing the input theory and a function q mapping embeddings of predictions into the space of \mathcal{M} . At regularization-time, LENSr maps via q the embedding of a $p(s,o)$ prediction into the space of \mathcal{M} , where the embedding of $p(s,o)$ is the sum of the word embeddings of s , p and o weighted by $w(p)$, $w(s)$ and $w(o)$. The L2 distance between the mapped embedding and \mathcal{M} serves as a loss to back-propagate through an SGG model. As the predictions of a model have higher uncertainty in scene graph classification than in predicate classification (not only p , but also s and o are now uncertain), the embedding of $p(s,o)$ will be further away from the prediction embeddings that LENSr has seen while learning q in advance of regularization. This discrepancy leads q to transform the prediction embeddings erroneously, leading to a loss function that provides a meaningless training signal. LENSr was not tested on scene graph classification by the authors (Xie et al. 2019).

Table 4: Impact of NGP(SL) on MOTIFS and VCTree with TDE. Results on the VG dataset.

Model	Theory	Reg.	Predicate Classification						Scene Graph Classification					
			mR@			zsR@			mR@			zsR@		
			20	50	100	20	50	100	20	50	100	20	50	100
MOTIFS	-	-	12.65	16.08	17.35	1.21	3.34	5.57	6.81	8.31	8.85	0.33	0.65	1.13
MOTIFS	-	TDE	17.18	23.95	27.66	8.10	13.68	17.11	10.11	13.44	15.35	1.85	3.01	3.68
MOTIFS	CNet ⁻	NGP(SL)+TDE	17.99	24.50	28.16	8.51	14.00	17.80	11.80	15.11	16.77	1.92	3.05	3.74
VCTree	-	-	13.07	16.75	18.11	1.04	3.28	5.52	9.29	11.42	12.12	0.48	1.37	2.09
VCTree	-	TDE	19.40	25.94	29.48	8.14	12.38	14.07	10.51	14.53	16.73	1.48	2.54	3.99
VCTree	CNet ⁻	NGP(SL)+TDE	23.91	30.78	34.19	8.15	12.47	15.41	13.60	17.69	19.85	1.57	2.63	3.63

Table 5: Impact of NGP(SL) and TDE on MOTIF when reducing the ground-truth facts from the OIv6 dataset.

% Red.	Reg.	Prd Cls mR@			Sg Cls mR@		
		20	50	100	20	50	100
-0%	-	45.62	46.10	46.15	28.83	28.90	28.92
-0%	TDE	41.85	42.00	42.01	12.80	12.87	12.87
-0%	NGP(SL)	48.15	48.65	48.70	25.79	26.07	26.10
-50%	-	42.63	43.12	43.17	25.75	25.81	25.83
-50%	TDE	31.91	32.07	32.08	19.31	19.34	19.36
-50%	NGP(SL)	45.93	46.41	46.46	25.92	26.21	26.24
-75%	-	41.97	42.16	42.17	23.21	23.27	23.28
-75%	TDE	33.93	34.09	34.10	14.67	14.73	14.74
-75%	NGP(SL)	44.40	44.90	44.94	24.94	25.23	25.26

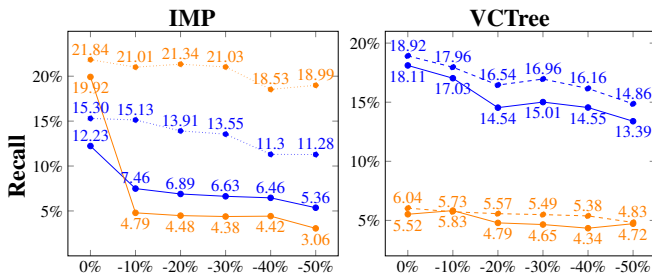


Figure 2: Impact of NGP on IMP and VCTree for predicate classification when reducing VG’s ground-truth. Blue lines show mR@100; orange show zR@100. Solid lines show mR and zSR w/o NGP; dotted show mR and zSR w/ NGP.

NGP complements bias reduction techniques. Regarding MOTIFS, the recall improvements brought by TDE are up to 59% and 73% in predicate and scene graph classification and increase to 62% and 89% when NGP is additionally applied using CNet⁻. Regarding VCTree, the recall improvements brought by TDE are up to 62% and 38% in predicate and scene graph classification; when NGP is additionally applied, recall increases up to 88% and 63%. Tables 2 and 4 show that the combination of TDE with NGP leads to much higher improvements than the sum of the improvements obtained by applying each technique separately.

NGP is particularly beneficial when reducing the amount of ground-truth facts. Figure 2 shows that the accuracy of SGG models can substantially decrease when reducing the ground-truth facts. In the case of VG, the most sensitive model is IMP: when reducing the training data by 50%, zsR@100 drops by more than 6.5 times (19.92 % vs. 3.06%), while mR@100 drops by more than two times (12.23 % vs. 5.36%). In the case of OIv6, Table 5, MO-

TIFS’ mR@100 drops from 46.15% to 42.17% in predicate classification when reducing the ground-truth by 75%; in scene graph classification, MOTIFS’ mR@100 drops from 28.92% to 23.28%. NGP can lead to drastic accuracy improvements for those cases. Regarding IMP and VG, zsR@100 can increase from 3.06% to 18.99% when reducing the ground-truth by 50%; zsR@100 can similarly increase from 5.36% to 11.28%. Similarly, when reducing by 75% of the ground-truth of OIv6, mR@100 for predicate classification can increase from 42.17% to 44.94% in the case of MOTIFS; mR@100 can increase from 42.17% to 44.94% for scene graph classification, when NGP is applied.

While NGP drops the mR of MOTIFS in scene graph classification when the whole ground-truth is used in OIv6, it is beneficial when reducing the ground-truth by 50% and 75%, Table 5. The high mR for MOTIFS even with significantly fewer ground-truth facts in Table 5 manifests that frequency-based techniques are effective for the OIv6 dataset. Still, the integration with logic-based approaches (NGP) can further improve mR, Table 5. It is also worth noting that while TDE is particularly effective in VG, it decreases the mR of MOTIFS up to 11% in OIv6. This is because OIv6 has a much higher annotation quality, and hence de-biasing is not crucial. Finally, in contrast to NGP, TDE provides no supervision when reducing the ground-truth facts.

Regularization can be more effective than sophisticated (neurosymbolic) SGG models. The mR@k of KBFN is 17.01% and 18.43% for predicate classification, see Figure 3. When jointly regularizing VCTree using NGP(SL) and TDE, the mR@k is 30.78% and 34.19%. Similarly, for scene graph generation, the mR@k of KBFN is 15.79% and 17.07%, and 17.69% and 19.85% for the regularized VCTree model. Likewise, the regularized VCTree model reaches up to 90% higher performance than BGNN. These results show that regularizing a standard SGG model like VCTree, can be more effective than ad-hoc, neurosymbolic SGG architectures or more sophisticated models.

Related work

Regularising neural models using symbolic knowledge has been extensively studied in information and natural language analysis (Wang and Pan 2020; Minervini and Riedel 2018; Rocktäschel, Singh, and Riedel 2015). Unlike the above line of research, NGP focuses on scalable knowledge injection into SGG models under different semantics.

Differently from contrastive learning (Oord, Li, and Vinyals 2018; Chen and He 2021; Jaiswal et al. 2021) where models are trained in an unsupervised fashion by perform-

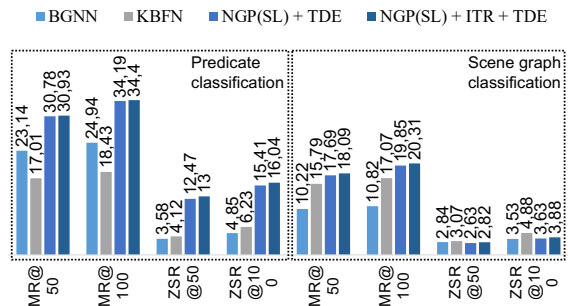


Figure 3: Regularization vs. ad-hoc architectures and sophisticated models. Results on the VG dataset.

ing tasks that can be created from the input itself, NGP trains neural models using symbolic domain knowledge. The authors in (Suhail et al. 2021) train a graph neural network to learn the joint conditional density of a scene graph and then use it as a loss function. To deal with the ambiguity in the SGG annotations, the work in (Yang et al. 2021) generates different probabilistic representations of the predicates. In contrast to NGP, the above techniques do not support external knowledge. Finally, the work in (Zhong et al. 2021) generates localized scene graphs from image-text pairs; the technique does not rely on logic, but exclusively on neural models. Integrating logic-based regularization with the above research is an interesting future direction.

Every technique that uses learned or fixed background knowledge as a prior, e.g., (Gu et al. 2019; Zareian et al. 2020), is biased towards that knowledge. Differently from techniques like MOTIFS (Zellers et al. 2018), NGP is not biased by the frequency of the training facts: if the background knowledge is independent of the training facts or their frequencies, then NGP will not be biased toward the training facts or their frequencies. The above holds as both the logic-based losses and NGP’s mechanism for choosing the maximally violated ICs are indifferent to any frequencies.

Conclusions

We introduced NGP, the first highly-scalable, symbolic, SGG regularization framework that leads to state-of-the-art accuracy. Future research includes supporting richer formulas and regularizing models under theories mined via knowledge extraction e.g., (Zhu, Fathi, and Fei-Fei 2014)– NGP supports such theories by weighting the ICs. Integrating NGP with neurosymbolic techniques that support indirect supervision like DeepProbLog (Manhaeve et al. 2018), NeuroLog (Tsamoura, Hospedales, and Michael 2021) and ABL (Dai et al. 2019) is another direction for future research.

References

Bach, S. H.; Broecheler, M.; Huang, B.; and Getoor, L. 2017. Hinge-Loss Markov Random Fields and Probabilistic Soft Logic. *Journal of Machine Learning Research*, 18: 109:1–109:67.

Chavira, M.; and Darwiche, A. 2008. On probabilistic inference by weighted model counting. *Artificial Intelligence*, 172(6): 772 – 799.

Chen, T.; Yu, W.; Chen, R.; and Lin, L. 2019. Knowledge-embedded routing network for scene graph generation. In *Proceedings of the IEEE/CVF Conference on Computer Vision and Pattern Recognition*, 6163–6171.

Chen, X.; and He, K. 2021. Exploring simple siamese representation learning. In *CVPR*, 15750–15758.

Dai, W.-Z.; Xu, Q.; Yu, Y.; and Zhou, Z.-H. 2019. Bridging Machine Learning and Logical Reasoning by Abductive Learning. In *NeurIPS*, 2815–2826.

Dao, T.; Kamath, G. M.; Syrgkanis, V.; and Mackey, L. 2021. Knowledge Distillation as Semiparametric Inference. In *ICLR*.

d’Avila Garcez, A. S.; Broda, K.; and Gabbay, D. M. 2002. *Neural-symbolic learning systems: foundations and applications*. Perspectives in neural computing. Springer.

Donadello, I.; Serafini, L.; and d’Avila Garcez, A. S. 2017. Logic Tensor Networks for Semantic Image Interpretation. In *IJCAI*, 1596–1602.

Fischer, M.; Balunovic, M.; Drachler-Cohen, D.; Gehr, T.; Zhang, C.; and Vechev, M. T. 2019. DL2: Training and Querying Neural Networks with Logic. In *ICML*, volume 97, 1931–1941.

Gu, J.; Zhao, H.; Lin, Z.; Li, S.; Cai, J.; and Ling, M. 2019. Scene Graph Generation With External Knowledge and Image Reconstruction. In *CVPR*, 1969–1978.

Hájek, P.; Godo, L.; and Esteva, F. 2013. Fuzzy Logic and Probability. *CoRR*, abs/1302.4953.

Hinton, G. E.; Vinyals, O.; and Dean, J. 2015. Distilling the Knowledge in a Neural Network. *CoRR*, abs/1503.02531.

Jaiswal, A.; Babu, A. R.; Zadeh, M. Z.; Banerjee, D.; and Makedon, F. 2021. A Survey on Contrastive Self-Supervised Learning. *Technologies*, 9(1).

Kendall, A.; Gal, Y.; and Cipolla, R. 2018. Multi-Task Learning Using Uncertainty to Weigh Losses for Scene Geometry and Semantics. In *CVPR*.

Krishna, R.; Zhu, Y.; Groth, O.; Johnson, J.; Hata, K.; Kravitz, J.; Chen, S.; Kalantidis, Y.; Li, L.; Shamma, D. A.; Bernstein, M. S.; and Fei-Fei, L. 2017. Visual Genome: Connecting Language and Vision Using Crowdsourced Dense Image Annotations. *Int. J. Comput. Vis.*, 123(1): 32–73.

Kuznetsova, A.; Rom, H.; Alldrin, N.; Uijlings, J. R. R.; Krasin, I.; Pont-Tuset, J.; Kamali, S.; Popov, S.; Mallocci, M.; Kolesnikov, A.; Duerig, T.; and Ferrari, V. 2020. The Open Images Dataset V4. *International Journal of Computer Vision*, 128(7): 1956–1981.

Li, R.; Zhang, S.; Wan, B.; and He, X. 2021. Bipartite Graph Network With Adaptive Message Passing for Unbiased Scene Graph Generation. In *CVPR*, 11109–11119.

Lu, C.; Krishna, R.; Bernstein, M.; and Fei-Fei, L. 2016. Visual Relationship Detection with Language Priors. In *ECCV*.

Manhaeve, R.; Dumancic, S.; Kimmig, A.; Demeester, T.; and De Raedt, L. 2018. DeepProbLog: Neural Probabilistic Logic Programming. In *NeurIPS*, 3749–3759.

- Minervini, P.; and Riedel, S. 2018. Adversarially Regularising Neural NLI Models to Integrate Logical Background Knowledge. In *CoNLL*, 65–74.
- Oord, A. v. d.; Li, Y.; and Vinyals, O. 2018. Representation learning with contrastive predictive coding. *arXiv:1807.03748*.
- Ren, S.; He, K.; Girshick, R.; and Sun, J. 2015. Faster R-CNN: Towards Real-Time Object Detection with Region Proposal Networks. In *NeurIPS*.
- Rocktäschel, T.; Singh, S.; and Riedel, S. 2015. Injecting Logical Background Knowledge into Embeddings for Relation Extraction. In *ACL*, 1119–1129.
- Sap, M.; Bras, R. L.; Allaway, E.; Bhagavatula, C.; Lourie, N.; Rashkin, H.; Roof, B.; Smith, N. A.; and Choi, Y. 2019. ATOMIC: An Atlas of Machine Commonsense for If-Then Reasoning. In *AAAI*, 3027–3035.
- Speer, R.; Chin, J.; and Havasi, C. 2017. ConceptNet 5.5: An Open Multilingual Graph of General Knowledge. In *AAAI*, 4444–4451.
- Suhail, M.; Mittal, A.; Siddiquie, B.; Broaddus, C.; Eledath, J.; Medioni, G. G.; and Sigal, L. 2021. Energy-Based Learning for Scene Graph Generation. In *CVPR*, 13936–13945.
- Tang, K. 2020. A Scene Graph Generation Codebase in PyTorch. <https://github.com/KaihuaTang/Scene-Graph-Benchmark.pytorch>.
- Tang, K.; Niu, Y.; Huang, J.; Shi, J.; and Zhang, H. 2020. Unbiased Scene Graph Generation From Biased Training. In *CVPR*, 3713–3722.
- Tang, K.; Zhang, H.; Wu, B.; Luo, W.; and Liu, W. 2019. Learning to Compose Dynamic Tree Structures for Visual Contexts. In *CVPR*, 6619–6628.
- Tsamoura, E.; Hospedales, T.; and Michael, L. 2021. Neural-Symbolic Integration: A Compositional Perspective. In *AAAI*.
- van Krieken, E.; Acar, E.; and van Harmelen, F. 2019. Semi-Supervised Learning using Differentiable Reasoning. *IF-CoLog Journal of Logic and its Applications*, 6(4): 633–653.
- van Krieken, E.; Acar, E.; and van Harmelen, F. 2020. Analyzing Differentiable Fuzzy Implications. In *KR*, 893–903.
- Wang, W.; and Pan, S. J. 2020. Integrating Deep Learning with Logic Fusion for Information Extraction. In *AAAI*, 9225–9232.
- Xie, Y.; Xu, Z.; Meel, K. S.; Kankanhalli, M. S.; and Soh, H. 2019. Embedding Symbolic Knowledge into Deep Networks. In *NeurIPS*, 4235–4245.
- Xu, D.; Zhu, Y.; Choy, C. B.; and Fei-Fei, L. 2017. Scene Graph Generation by Iterative Message Passing. In *CVPR*, 3097–3106.
- Xu, J.; Zhang, Z.; Friedman, T.; Liang, Y.; and Van den Broeck, G. 2018. A Semantic Loss Function for Deep Learning with Symbolic Knowledge. In *ICML*, 5502–5511.
- Yang, G.; Zhang, J.; Zhang, Y.; Wu, B.; and Yang, Y. 2021. Probabilistic Modeling of Semantic Ambiguity for Scene Graph Generation. In *CVPR*, 12527–12536.
- Zareian, A.; Karaman, S.; and Chang, S.-F. 2020. Bridging Knowledge Graphs to Generate Scene Graphs. In *ECCV*.
- Zareian, A.; Wang, Z.; You, H.; and Chang, S.-F. 2020. Learning Visual Commonsense for Robust Scene Graph Generation. In *ECCV*, 642–657.
- Zellers, R.; Yatskar, M.; Thomson, S.; and Choi, Y. 2018. Neural Motifs: Scene Graph Parsing With Global Context. In *CVPR*, 5831–5840.
- Zhang, H.; Kyaw, Z.; Chang, S.; and Chua, T. 2017. Visual Translation Embedding Network for Visual Relation Detection. In *CVPR*, 3107–3115.
- Zhong, Y.; Shi, J.; Yang, J.; Xu, C.; and Li, Y. 2021. Learning to Generate Scene Graph from Natural Language Supervision. In *ICCV*, 1803–1814.
- Zhu, Y.; Fathi, A.; and Fei-Fei, L. 2014. Reasoning about Object Affordances in a Knowledge Base Representation. In *ECCV*, volume 8690, 408–424.

Appendix

Adapting Logic Tensor Networks for our analysis

LTNs is a neurosymbolic framework (Donadello, Serafini, and d’Avila Garcez 2017). The framework was applied to the task of predicting whether the objects enclosed in specific bounding boxes adhere to the `partOf` relation. In this section, we present how we extended LTNs for predicate and scene graph classification in our experimental setup.

Background LTNs consists of two parts: a neural model n for object classification and, on top of n , a logical theory T that reasons in a symbolic fashion over the predictions of n . In the setting presented in (Donadello, Serafini, and d’Avila Garcez 2017), theory T outputs facts of the form $\circ(b)$ and $\text{partOf}(b_1, b_2)$ denoting that the object within bounding box b is of type \circ and that the object within b_1 is a part of the object within b_2 , respectively. The semantics of T is defined through a class of interpretation functions \mathcal{G} mapping each fact to the $[0, 1]$ interval. In particular, the confidence of a fact $\circ(b)$ is given by $\mathcal{G}(\circ)(b)$, while the confidence of a fact $\text{partOf}(b_1, b_2)$ is given by $\mathcal{G}(\text{partOf})(b_1, b_2)$, where $\mathcal{G}(\circ)$ and $\mathcal{G}(\text{partOf})$ are functions from bounding boxes² and pairs of bounding boxes into $[0, 1]$. Intuitively, the functions in \mathcal{G} reflect the degree to which the *entire* framework has certain beliefs on the types of the objects or their inter-relationships. To accommodate logical theories, \mathcal{G} additionally includes functions for interpreting formulas in first order logic using the semantics of Lukasiewicz’s fuzzy logic:

$$\mathcal{G}(\neg\varphi) := 1 - \mathcal{G}(\varphi) \quad (10)$$

$$\mathcal{G}(\varphi_1 \wedge \varphi_2) := \max\{0, \mathcal{G}(\varphi_1) + \mathcal{G}(\varphi_2) - 1\} \quad (11)$$

$$\mathcal{G}(\varphi_1 \vee \varphi_2) := \min\{1, \mathcal{G}(\varphi_1) + \mathcal{G}(\varphi_2)\} \quad (12)$$

Above, φ , φ_1 and φ_2 are formulas over variables and the Boolean connectives \wedge , \vee and \neg . The aim of LTNs is to learn the weights of the neural model so that \mathcal{G} correctly predicts (i) the object within a bounding box, as well as (ii) whether two objects described in terms of their surrounding bounding boxes abide by the `partOf` relation. Regularization of the neural model is achieved via \mathcal{G} , in the sense that the model’s weights are changed so that the outputs of \mathcal{G} satisfy the background knowledge as well as agree with the annotations in the ground truth. Below, we discuss how we used LTNs for predicate and scene graph classification. Before that, notice that the neural SGG models provide two interfaces. Given a bounding box b , the first interface outputs the confidence to which the object enclosed in b belongs to a class \circ in \mathcal{O} . Given two bounding boxes b and b' , the second interface outputs the confidence to which the objects enclosed in b and b' relate according to a predicate \mathfrak{p} in \mathcal{P} . Furthermore, to establish a fair comparison we used the neural model from (Ren et al. 2015) for object detection.

We are now ready to describe our extension. The first step is to extend \mathcal{G} with functions for object and predicate classification. These functions classify an object (resp. pair of

²LTNs represent bounding boxes using their upper left and lower right coordinates in the image.

objects) to an object class \circ (resp. predicate class \mathfrak{p}), if \circ (resp. \mathfrak{p}) is assigned the maximum confidence by the neural model. In particular, following (Donadello, Serafini, and d’Avila Garcez 2017), we added to \mathcal{G} a function $\mathcal{G}(\circ_i)$, for each $\circ_i \in \mathcal{O}$, which outputs 1 if the object enclosed in the input bounding box is of type \circ_i , and 0, otherwise. Furthermore, for each $\mathfrak{p}_i \in \mathcal{P}$, we added a function $\mathcal{G}(\mathfrak{p}_i)$, which, given a pair of bounding boxes b and b' , takes value 1 if the most likely predicate describing the relationship between b and b' is \mathfrak{p}_i according to the neural model, and 0, otherwise.

The second step is to add the background theory, while the final step is to create training data³. We followed the procedure described in (Donadello, Serafini, and d’Avila Garcez 2017). For each bounding box b_i annotated with the object class \circ_i , we added the fact $\circ_i(b_i)$, as well as the facts $\neg\circ_j(b_i)$, for each $j \neq i$. Furthermore, for each pair of bounding boxes (b_i, b_j) annotated with predicate \mathfrak{p} , we added the fact $\mathfrak{p}(b_i, b_j)$, as well as the facts $\neg\mathfrak{p}'(b_i, b_j)$, for each $\mathfrak{p}' \neq \mathfrak{p}$. All facts in the training set have confidence 1. Provided with all this information, LTNs train the neural SGG model.

Implementation Details & Additional Results

Implementation details We used the state of the art open source library from (Tang 2020) (released under the MIT license) for implementing all neural SGG models considered in our evaluation. The library fixes bugs affecting previous implementations that were leading to very high results. This is why the reported results may differ from the ones in previously published work.

To ensure a fair comparison and following the widely adopted protocol in literature, we used the same pre-trained Faster R-CNN (Ren et al. 2015) backbone for object detection⁴ for all models following the procedure from (Tang et al. 2020) for training it. We train the SGG models of IMP, MOTIFS and VCTree using SGD, with a batch size of 12, a learning rate of 1×10^{-2} , and a weight decay of 1×10^{-4} , keeping the hyperparameters recommended by the authors.

For the experiments with OIv6, we used for all models the same pre-trained Faster R-CNN with the experiments with VG. The hyperparameters presented above are also used for the OIv6 dataset, following the evaluation procedure by (Li et al. 2021). To evaluate BGNN, we used the implementation⁵ provided by the authors (Li et al. 2021). It should be stressed that the results reported for BGNN in (Li et al. 2021) are not reproducible with the codebase provided by the authors. This is an ongoing issue that has been also reported by the other users of the codebase.

To compute SL, we used the PySDD library version 0.2.10 (licensed under the Apache License, version 2.0) that compiles formulas into arithmetic circuits.

³The VG benchmark annotates each pair of bounding boxes (b_i, b_j) in the ground truth with the types \circ_i and \circ_j of the enclosed objects, and the predicate \mathfrak{p} describing their relationship.

⁴For predicate and scene graph classification, Faster R-CNN acts only as a feature extractor.

⁵Available at <https://github.com/Scarecrow0/BGNN-SGG> under the MIT license.

Additional results

NGP is time-efficient Table 6 reports results on VCTree with TDE when increasing the number of the ICs used by NGP. The benchmark is VG. We used this model combination as it leads to the highest recall in our previous analysis. The Time column reports the time in seconds for processing 200 batches of size 12 using two NVidia GeForce GTX 1080 Ti GPUs. Table 6 shows that the overhead to compute (8) at each training step is small in practice: the runtime tends to increase linearly with the number ρ of ICs.

Table 6 shows that both for predicate classification and scene graph classification, the recall may drop by increasing ρ . We conjecture that this is due to the extreme bias and inaccuracies in the ground-truth in VG, a phenomenon already known to the community (Tang et al. 2020). In an unbiased dataset, the recall is expected to increase when the knowledge becomes richer (e.g., by increasing the number of ICs in our case) as the supervision signal becomes stronger. However, in the case of extreme bias, a more accurate model may not have the best recall. For instance, in quite a few cases, the ground-truth facts use the predicate `on`, despite that `laying on` better describes the relationship between the subject and the object. If a model is more accurate towards detecting the `laying on` relation, then some detections of `laying on` will be mistakenly considered as wrong ones dropping the recall measures.

Randomly chosen ICs can drop recall Table 7 repeats the experiment from Table 6, by randomly choosing the ICs this time, though. The random selection technique leads to generally lower recall than the greedy technique proposed in Algorithm 2, while for zero-shot recall, the recall is consistently lower than that reported in Table 6. This highlights the effectiveness of our proposed strategy.

NGP is effectively integrated with TDE Table 8 reports results for NGP(SL) and GLAT on VCTree in combination with TDE. The benchmark is VG. In contrast to Table 4, NGP is applied using VG^- to establish a fair comparison against GLAT by using knowledge exclusively coming from the training data. We can see that, in contrast to NGP, GLAT can substantially drop the recall of the model when employed in conjunction with TDE. For instance, mR@k drops from 19.40%, 25.94% and 29.48% to 13.07%, 19.05% and 23.14%. In contrast to GLAT, NGP improves the recall of the model in most cases. Regarding predicate classification, mR@k increases to 24.07%, 31.06% and 34.53%, while regarding scene graph classification, mR@k increases to 11.19%, 15.10% and 17.66%. We plan to investigate the cases where zsR@k drops for predicate classification.

BGNN is sensitive to regularization As discussed in the main body of the paper, the sampling-based approach of BGNN makes its integration with regularization based techniques difficult. Table 9 presents results on the integration of BGNN with GLAT, LENSr and NGP. We can see that GLAT has no impact on BGNN in predicate classification, while it drops its accuracy in scene graph classification. LENSr, in turn, drops both the mR and zsR for predicate classification in most cases improving only mR for scene

graph classification. Overall, NGP is the most effective regularization technique as shown in Table 9: it leads to substantial improvements in zsR and mR in predicate and scene graph classification, respectively, dropping the recall in the remaining cases, though.

NGP improves recall for less frequent predicates Figure 4 shows the frequency of ground-truth facts in VG grouped by their predicates. The long tail effect becomes immediately apparent as the majority of predicates is used in less than 10% of the ground-truth. For instance, the number of ground-truth facts having the `on` and `has` predicates is substantially higher than the number of facts having the `flying on` predicate.

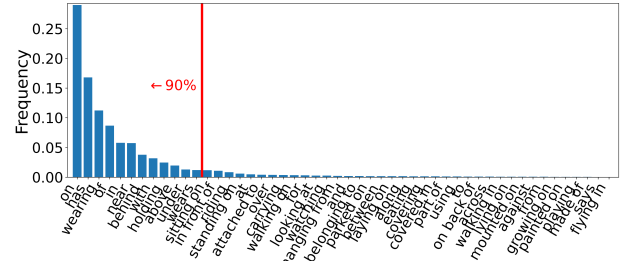


Figure 4: Frequency of the ground-truth facts in VG grouped by their predicates.

Figures 5 and 6 show results on mR@100 on a per-predicate basis for predicate and scene graph classification. The benchmark is VG. Regularization is performed using NGP(SL) with CNet^- and $\rho = 2$. The relative recall improvements can be substantial. NGP can be seen as a form of weak supervision, where the model is provided with feedback that comes from ICs encoding commonsense knowledge in addition to the training signal that comes from the image labels. Intuitively, this signal can be seen as a way to help the model in better learning the less frequent predicates as for the more frequent ones there is already plenty of signal from the labelled data. A model trained only with the ground-truth would lack this signal.

It is worth noting that the baseline recall may drop for the frequent predicates in some cases. This is due to inaccuracies in the ground truth (Tang et al. 2020) making the vast majority of the ground truth facts erroneously referencing only very few predicates, see Figure 4. For instance, in quite a few cases, the ground truth facts use the predicate “on”, even when “laying on” better describes the relationship between the subject and the object. Due to inaccuracies in the ground truth, the recall of a model that is more effective in detecting less frequent predicates, may be erroneously reported lower for the more frequent predicates.

Table 6: Impact of the number of ICs on NGP’s accuracy. Results on the VG dataset.

Model	Theory	Regularization	# ICs	Predicate Classification						Scene Graph Classification							
				mR@			zsR@			Time (s)	mR@			zsR@			Time (s)
				20	50	100	20	50	100			20	50	100	20	50	
VCTree	-	TDE	0	19.40	25.94	29.48	8.14	12.38	14.07	330.85	10.51	14.53	16.73	1.48	2.54	3.99	370.22
VCTree	CNet [⊥]	NGP(SL)+TDE	2	23.91	30.78	34.19	8.15	12.47	15.41	367.14	13.60	17.69	19.85	1.57	2.63	3.63	437.44
VCTree	CNet [⊥]	NGP(SL)+TDE	3	23.99	31.31	35.10	6.72	10.61	13.36	389.29	13.18	17.23	19.42	1.67	3.00	3.95	617.89
VCTree	CNet [⊥]	NGP(SL)+TDE	5	23.90	31.22	35.17	6.81	10.69	13.24	487.04	13.50	17.31	19.70	2.74	4.09	5.12	725.62
VCTree	CNet [⊥]	NGP(SL)+TDE	7	24.75	32.14	35.82	7.17	10.81	13.68	540.01	12.57	17.22	19.33	1.64	2.93	3.59	834.85
VCTree	CNet [⊥]	NGP(SL)+TDE	10	24.32	31.59	35.11	6.10	10.52	13.26	606.95	12.29	17.15	19.26	1.68	2.94	3.83	983.34

Table 7: Impact of randomly chosen ICs. Results on the VG dataset.

Model	Theory	Regularization	# ICs	Predicate Classification						Scene Graph Classification						
				mR@			zsR@			mR@			zsR@			
				20	50	100	20	50	100		20	50	100	20	50	100
VCTree	CNet [⊥]	TDE	0	19.40	25.94	29.48	8.14	12.38	14.07	10.51	14.53	16.73	1.48	2.54	3.99	
VCTree	CNet [⊥]	NGP(SL)+TDE	2	23.86	31.14	34.66	6.53	10.61	13.13	11.97	16.23	18.53	3.54	5.46	6.81	
VCTree	CNet [⊥]	NGP(SL)+TDE	3	23.99	31.33	34.91	6.57	10.63	13.70	12.60	16.61	19.08	3.53	5.27	6.87	
VCTree	CNet [⊥]	NGP(SL)+TDE	5	24.31	31.46	35.25	6.57	10.29	13.03	12.76	16.94	19.30	3.75	5.37	7.00	
VCTree	CNet [⊥]	NGP(SL)+TDE	7	23.63	30.85	34.58	6.57	10.38	13.14	10.92	15.30	17.71	3.04	4.93	6.47	
VCTree	CNet [⊥]	NGP(SL)+TDE	10	10.93	14.16	15.45	5.16	9.90	13.49	10.90	15.27	17.67	3.02	4.91	6.49	

Table 8: Impact of GLAT and NGP on VCTree with TDE. Results on the VG dataset.

Model	Theory	Regularization	Predicate Classification						Scene Graph Classification						
			mR@			zsR@			mR@			zsR@			
			20	50	100	20	50	100		20	50	100	20	50	100
VCTree	-	TDE	19.40	25.94	29.48	8.14	12.38	14.07	10.51	14.53	16.73	1.48	2.54	3.99	
VCTree	VG [⊥]	NGP(SL)+TDE	24.07	31.06	34.53	6.30	10.46	12.90	11.19	15.10	17.66	1.66	2.64	3.51	
VCTree	-	TDE	19.40	25.94	29.48	8.14	12.38	14.07	10.51	14.53	16.73	1.48	2.54	3.99	
VCTree	-	GLAT+TDE	13.07	19.05	23.14	4.99	8.09	11.01	0.90	2.06	3.60	1.30	2.22	3.18	

Table 9: Impact of different regularization techniques on BGNN’s accuracy. Results on the VG dataset.

Model	Theory	Regularization	Predicate Classification						Scene Graph Classification						
			mR@			zsR@			mR@			zsR@			
			20	50	100	20	50	100		20	50	100	20	50	100
BGNN	-	-	19.07	23.14	24.94	1.86	3.58	4.85	8.7	10.22	10.82	1.71	2.84	3.53	
BGNN	-	GLAT	19.07	23.14	24.94	1.86	3.58	4.85	5.53	7.19	8.06	0.66	1.14	1.69	
BGNN	-	-	19.07	23.14	24.94	1.86	3.58	4.85	8.7	10.22	10.82	1.71	2.84	3.53	
BGNN	CNet [⊥]	LENSR	18.55	22.74	24.50	1.98	3.44	4.86	10	12.44	13.39	1.41	2.04	2.58	
BGNN	-	-	19.07	23.14	24.94	1.86	3.58	4.85	8.7	10.22	10.82	1.71	2.84	3.53	
BGNN	CNet [⊥]	NGP(SL)	17.41	21.38	22.91	2.43	4.52	6.53	9.39	11.23	11.98	1.66	2.78	3.53	

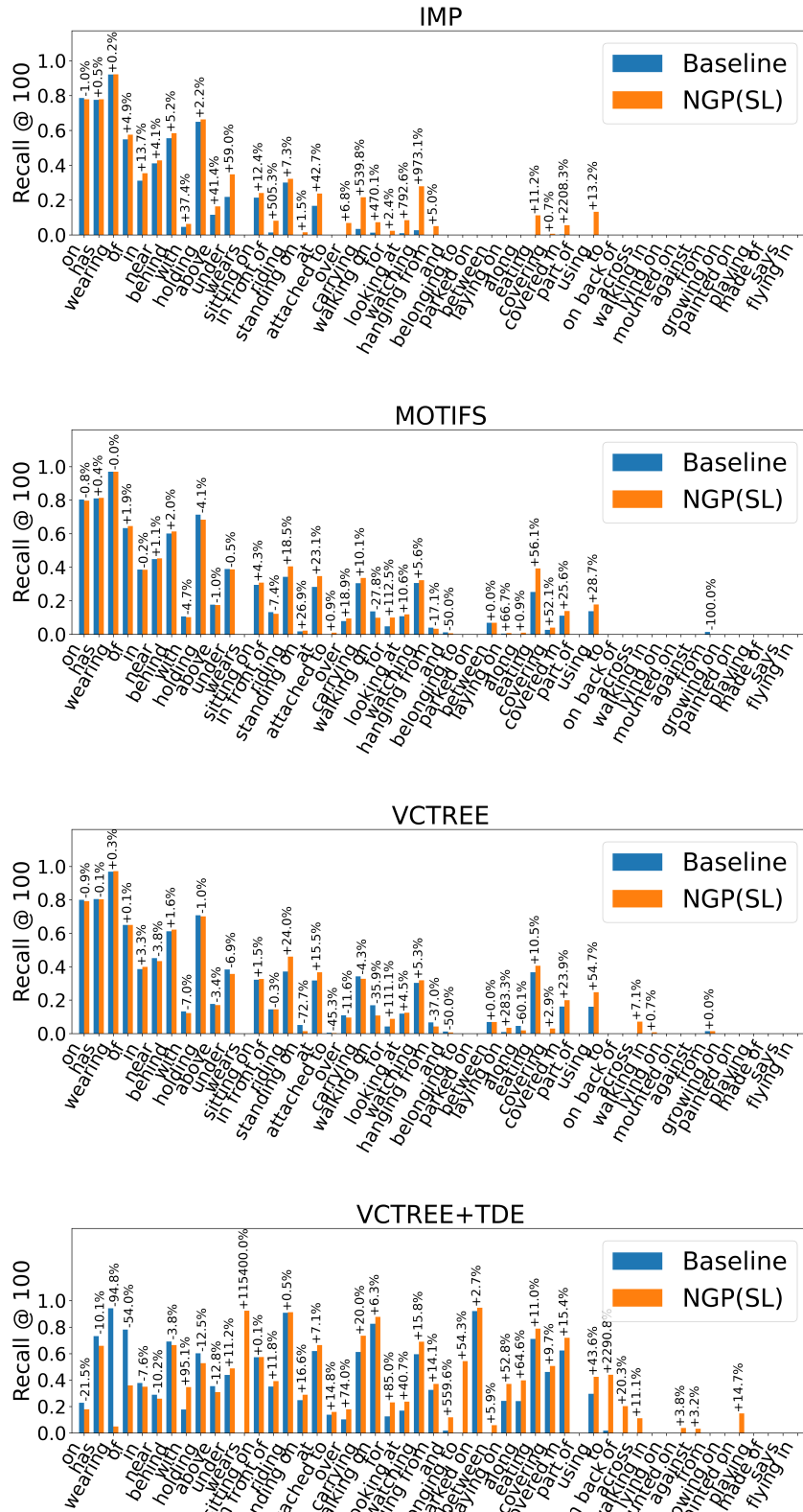


Figure 5: Recall for predicate classification on a per-predicate basis. Results on the VG dataset.

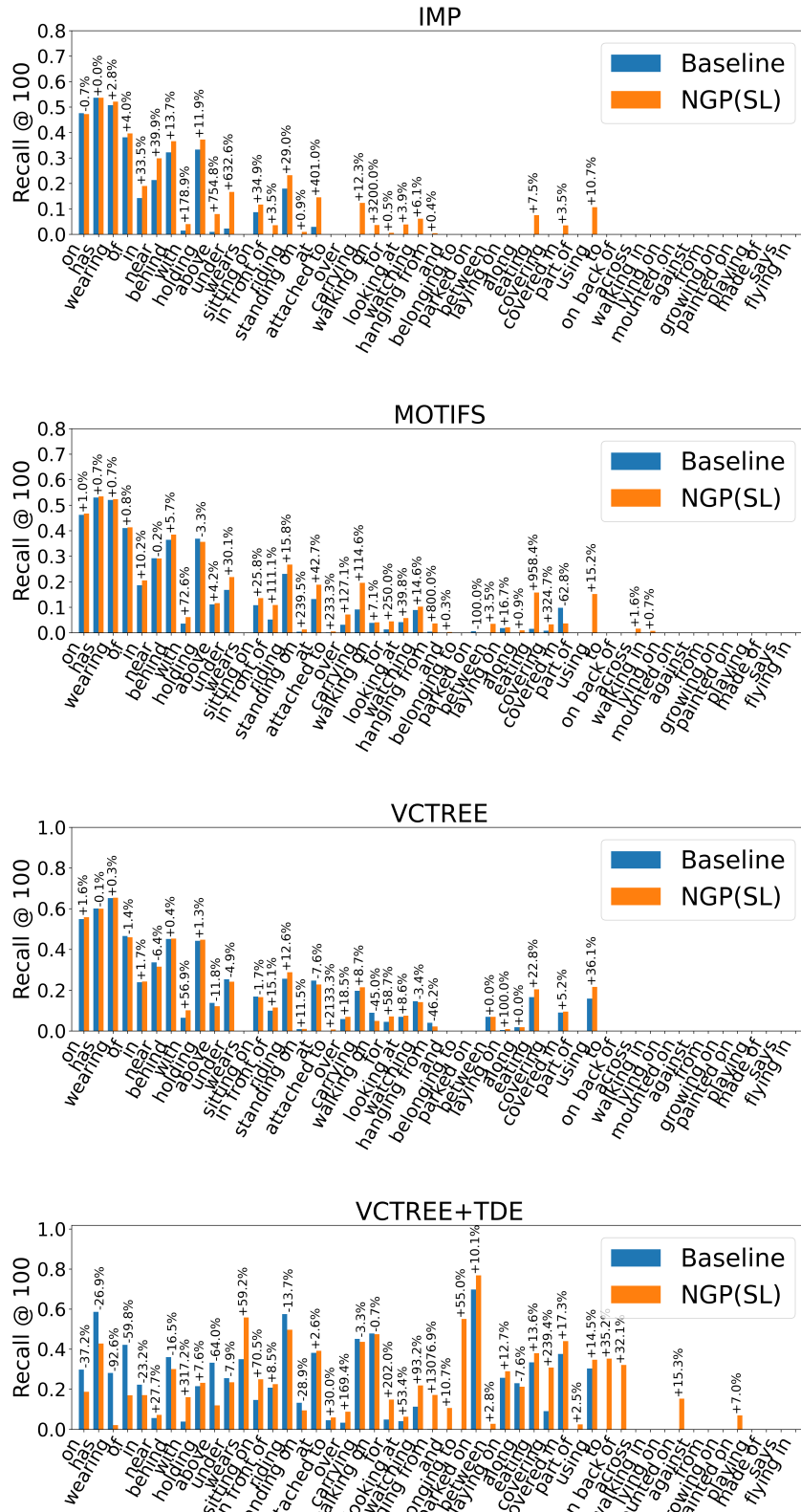


Figure 6: Recall for scene graph classification on a per-predicate basis. Results on the VG dataset.